# RECENT DEVELOPMENTS IN ENGINEERING DESIGN FOR THE QUASI-AXISYMMETRIC STELLARATOR CFQS

A. Shimizu[1,2], S. Kinoshita[1], M. Isobe[1,2], S. Okamura[1], K. Ogawa[1,2], M. Nakata[1,2], Y. Yoshimura[1],
C. Suzuki[1,2], M. Osakabe[1,2], T. Murase[1], S. Nakagawa[1], H. Tanoue[1],
Y. Xu[3], H. F. Liu[3], H. Liu[3], J. Huang[3], X. Wang[3], J. Cheng[3], G. Xiong[3], C. Tang[4], D. Yin[5], Y. Wan[5]

*1) National Institute for Fusion Science, National Institutes of Natural Sciences, Toki, Gifu, Japan*
*2) The Graduate University for Advanced Studies, SOKENDAI, Toki, Gifu, Japan*
*3) Institute of Fusion Science, School of Physical Science and Technology, Southwest Jiaotong University, Chengdu, China*
*4) School of Physical Science and Technology, Sichuan University, Chengdu, China*
*5) Hefei Keye Electro Physical Equipment Manufacturing Co., Ltd, Hefei, China*

Email: shimizu.akihiro@nifs.ac.jp

## Abstract

A quasi-axisymmetric stellarator CFQS has been designed as a Joint project of National Institute for Fusion Science and Southwest Jiaotong University to prove intrinsic advantages of quasi-axisymmetry. Principal parameters of the CFQS are as follows: the major radius is 1 m, the magnetic field strength is 1 T, the aspect ratio is 4, and the toroidal periodic number is 2. Magnetic field configuration is designed based on that of CHS-qa. Enhanced confinement property in the context of neoclassical theory is achieved by its quasi-axisymmetric configuration. In entire radial range, magnetic well is retained to keep favorable stability features in MHD equilibrium. Magnetic field coil system was designed for the CFQS, which consists of 16 modular coils, 12 toroidal field coils, and 4 poloidal field coils. Supporting structure is designed to withstand strong electromagnetic force under 1 T operation, maintaining enough space for heating and diagnostic systems. The mock-up modular coil having the most complicated shape was constructed by Hefei Keye Electro Physical Equipment Manufacturing Co., Ltd. to check manufacturability, and the achieved accuracy. Heat run test was performed to check temperature rise of conductors, and the capability of 1 T operation was confirmed. After various tests for the mock-up coil, construction of actual modular coils and the vacuum vessel has begun.

## 1. INTRODUCTION

Helical devices are advantageous over tokamak in terms of steady-state operation capability as a future nuclear fusion reactor, because their magnetic field configurations are produced by external magnetic field coils and no inductive plasma current is intrinsically required. The neoclassical confinement of a standard helical device such as Compact Helical System (CHS [1]) deteriorates basically in the low collisional regime. This is because that when the collision frequency less than the precession frequency of trapped particles in helical ripples, the radial particle diffusion becomes large due to the drifts in this helical banana orbits. In this regime, the radial particle diffusion is proportional to $1/\nu$, here the $\nu$ is collisional frequency, so this is called as $1/\nu$ regime. In recent decades, to improve this disadvantage, various optimized stellarator configurations have been proposed, which have favourable neoclassical confinement features with improved magnetohydrodynamics (MHD) stability. Helically Symmetric Experiment (HSX [2]) and Wendelstein 7-X (W7-X [3-5]) were constructed as optimized stellarator devices, and plasma experiments have been conducted. A quasi-axisymmetric stellarator (QAS[6,7]) is one of those optimized stellarators, of which magnetic field strength $B$ is axisymmetric in a magnetic coordinate, *i.e.*, the Boozer coordinates [8]. In more precise definition, the QAS means that $B$ only depends on the poloidal angle of Boozer coordinates, and it is invariant along the toroidal angle like tokamaks. The neoclassical transport property of QAS is comparable to that of tokamaks. Moreover, the QAS requires no plasma current to confine a plasma, thus, the steady-state operation capability is retained. The CFQS [9-13] is the world's first quasi-axisymmetric stellarator, which is being constructed, under the international joint project of National Institute for Fusion Science (NIFS) in Japan and Southwest Jiaotong University (SWJTU) in China. Up to now, the mock-up modular coil was constructed by Hefei Keye Electro Physical Equipment Manufacturing Co., Ltd. to check manufacturability, and the achieved manufacturing accuracy. Subsequently, heat-run test was performed to check temperature rise of copper conductors, and as a result, the capability of 1 T operation was confirmed. Construction of actual modular coils and the vacuum vessel has begun. In this paper, recent progress of the physics, the engineering design, and construction status of the CFQS are described.

## 2. PHYSICS PROPERTY OF THE CFQS

Our research target of CFQS is to study the confinement and the turbulence physics of plasma in QAS experimentally, and to obtain beneficial knowledge to improve the performance of future reactor scale plasma. For this purpose, the target plasma temperature and density are order of keV and $10^{19}$ $m^{-3}$, respectively. Therefore, we chose the major radius ($R$) of 1 m, the magnetic field strength ($B_t$) of 1 T for CFQS. The large minor radius is required to achieve above plasma parameters, so the aspect ratio ($A_p$) of 4, and the toroidal periodic number ($N_p$) of 2 were chosen. The MHD equilibrium of CFQS was designed based on the CHS-qa [14-17]. $A_p$ of 4 is very low among stellarators in the world, and this low aspect ratio brings challenging issues in the engineering design of magnetic field coils and support structures. The geometry of plasma boundary on vacuum condition is shown in Fig. 1. The rotational transform profile is between 0.35 and 0.4 to avoid the low mode rational surface. In all radial region, the magnetic well property is achieved to stabilize MHD characteristics. The magnetic field strength, $B$, can be expressed as, $B = \Sigma B_{mn} \cos (m \theta + n N_p \zeta)$, in the Boozer coordinate. Here, $\theta$ and $\zeta$ are poloidal and toroidal angles, respectively. And $m$ and $n$ are poloidal and toroidal mode numbers. In Fig.2, radial profiles of 10 largest $B_{mn}$ are shown. In standard tokamak with circular cross section, the magnetic field strength can be expressed as follows, $B = R_0 B_0 / R = R_0 B_0 / (R_0 + r \cos \theta) = B_0 / ( 1 + \varepsilon_t \cos \theta) \sim B_0 ( 1 - \varepsilon_t \cos \theta)$. Here, $R$ and $r$ are major and minor radius, and $\varepsilon_t$ is the inverse aspect ratio of $r/R_0$. $R_0$ and $B_0$ are typical major radius and magnetic field strength of device. Therefore, $\varepsilon_t$ in tokamaks corresponds to $B_{10}$, which comes from the dependence of $B$ on $1/R$, and it means toroidicity. In Fig.2, $B_{10}$ is dominant like tokamak, therefore, neoclassical properties of CFQS are similar to tokamaks. The neoclassical diffusion coefficients are reduced sufficiently compared with CHS as shown in ref. [9]. Similar to tokamaks, large bootstrap current is expected. The bootstrap current estimated by BOOTSJ code [18,19] reaches about 30 kA at the volume-averaged beta ($<\beta>$) of 1 % [9]. In this bootstrap current estimation, the temperature profile is assumed to be parabolic, $T = T_0 (1 - s )$, and the density profile is relatively flat, i.e., $n = n_0 (1 - 0.8 s + 1.3 s^2 - 1.5 s^3 )$, where $s$ is normalized toroidal magnetic flux. For density, $n_0 = 1.0 \times 10^{19}$ $m^{-3}$, and $T_i = 0.75 T_e$ are assumed. The finite beta MHD equilibrium is calculated by HINT2 [20,21] as shown in Fig. 3. Poincare plots of magnetic field line at the toroidal angle of 0 deg. at $<\beta>$ of 0.8 and 1.2 % are shown. In this figure, green line shows the position of vacuum vessel. The neoclassical bootstrap current is taken into account in this equilibrium. Clear magnetic flux surfaces are sustained, at least up to $<\beta>$ of 1.2 %, which is attainable by neutral beam injection (NBI) heating in experiments. The effect of toroidal current and beta on degrading quasi-axisymmetry is small [9]. For stability, we discussed about Mercier criteria and ballooning stability [12]. Up to $<\beta>$ of 2 %, Mercier criteria shows stable. As for the ballooning stability, above $<\beta>$ 1.1 %, it becomes unstable, however, from $<\beta>$ of 2.7 %, second stability appears.

For the scenario to suppress anomalous transport and to achieve improved confinement, the plasma rotation is important. In tokamaks and helical systems, the formation of transport barriers were observed in experiments [22-24], and the physics of transport barrier formations is strongly related to plasma rotation and shear flow. The plasma rotation is determined by the balance between driving force and damping force of viscosity. The neoclassical viscosity of CFQS in toroidal direction is the same order of CHS-qa [25], which means it is very small, and it in poloidal direction is also small compared with CHS. This feature has advantage to drive large plasma rotation and produce shear flow for transport barrier formation. Actually, viscosity due to anomalous transport will be also important in experiments as discussed in CHS [26]. To clarify the relationship between the neoclassical viscosity, the plasma rotation, anomalous transport and improved confinement, the flexibility of magnetic field configuration is designed.

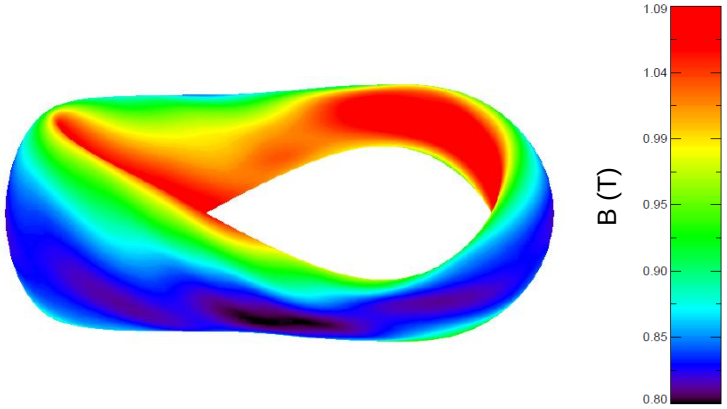


*Figure 1. Plasma boundary of CFQS. The color represents magnetic field strength.*

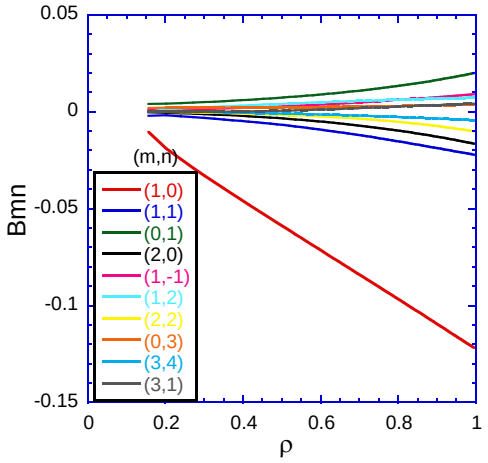


*Figure 2. Spectrum of Bmn in Boozer's coordinates.*

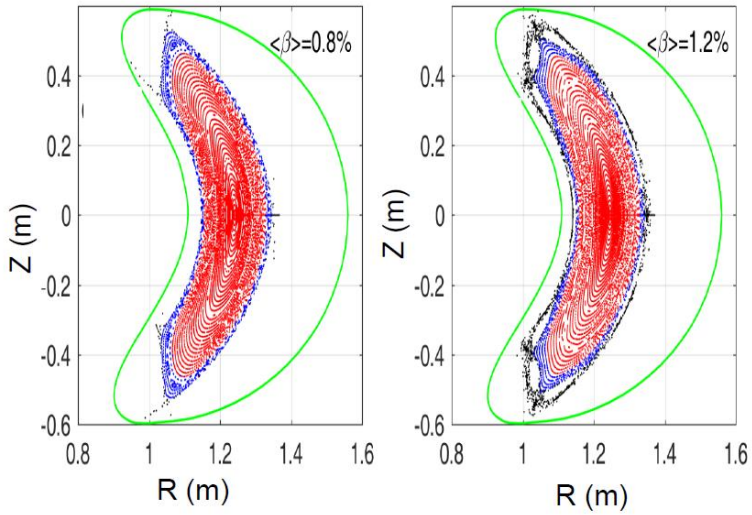


*Figure 3. Finite beta MHD equilibrium taking the neoclassical bootstrap current into account. Left: <β> of 0.8 %. Right: <β> of 1.2 %.*

## 3. EXPERIMENTAL PLAN

Although the final target in operational $B_t$ is 1 T, the CFQS will be operated in $B_t$ of 0.1 T in the initial phase of experiment. In this case, a CFQS plasma is produced by 2.45 GHz magnetron. The CW operation is possible for the case of 0.1 T, therefore, it is suitable for the mapping experiment to check the shapes of magnetic flux surfaces. Discharge cleaning for wall conditioning is also appropriate in this operation. For 1 T operation, electron cyclotron resonance heating (ECRH) with 54.5 GHz gyrotron used in CHS is employed to initiate plasma, of which injection power is approximately 450 kW [11]. The confinement performance of QA configuration in high-temperature plasma, in other words, in low collisional regime, will be studied. After the preparation of ECRH, the installation of NBI heating system used in CHS is also planned. Beam energy and heating power are 30 keV and 1 MW, respectively. Neutral beam (NB) will be tangentially injected, and deposition rate of NB reached 60 % at the line averaged density of $7 \times 10^{19}$ m$^{-3}$ from the HFREYA code calculation [27]. NBI allows us to access high-density plasma to study high-beta physics, and it can also be utilized to study high-energy particle confinement, and MHD stability driven by high-energy particles. Beam-driven current can work an additional knob to control rotational transform profile in experiments.

From the neoclassical point of view, QA configuration has tokamak-like good confinement without current drive. Note that in experiments, the anomalous transport caused by turbulence will be dominant. In the QA configuration, the transport barrier formation such as H-mode [22-23] in tokamaks will be expected due to its intrinsic low-viscosity. Therefore, we will study physics of improved confinement mode by measuring $E_r$, which plays an important role in transition to H-mode, and suppression of turbulence leading to confinement improvement. Heavy ion beam probe, so-called HIBP, used in CHS [24, 28] will be employed to study physics mentioned above. Doppler microwave reflectometer and charge exchange spectrometer will be also prepared as other methods to measure the profile of flow in the plasma.

From scaling of ISS95 [29], energy confinement time of stellarators, $\tau_{ISS95}$ (s), is expressed as, $0.079\ a^{2.21}\ R^{0.65}\ P^{-0.59}\ \bar{n}_e^{0.51}\ B_t^{0.83}\ t^{0.4}$. Here, $a$ (m): averaged minor radius, $R$ (m): major radius, $P$ (MW): heating power, $\bar{n}_e$ ($10^{19}$ m$^{-3}$) : line averaged density, $B_t$ (T): toroidal magnetic field strength, $t^{0.4}$: rotational transform. Expected plasma parameters of CFQS estimated from this are shown in Fig. 4. In this calculation, for profiles, same assumptions in section 2 are considered, namely, $T = T_0\ (1 - s\ )$, $T_i = 0.75\ T_e$, and $n = n_0\ (1 - 0.8\ s + 1.3\ s^2 - 1.5\ s^3\ )$. In low density case, $n_0 = 1.0 \times 10^{19}$ m$^{-3}$, temperature dependence on heating power is shown in Fig. 4 (a). In this Fig.4, *Hf* means the improved factor from ISS95 scaling, which is scanned from 1 to 2. $T_{e0}$ of 1 keV will be achieved so low collisional regime can be accessed. In Fig.4 (b), volume averaged β as a function of heating power are shown in the case of high density, $n_0 = 5.0 \times 10^{19}$ m$^{-3}$. Heating power of 1 MW, at least $<\beta>$ of 1 % is expected from this estimation.

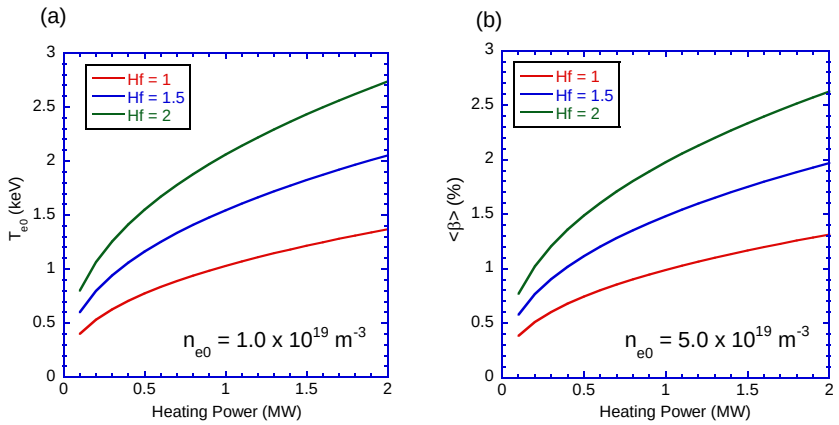


*Figure 4. (a) Central temperature dependence on the heating power in CFQS estimated from ISS95 scaling low. (b) Volume averaged $\beta$ dependence on heating power. For profiles, $T = T_0\ (1 - s\ )$, $T_i = 0.75\ T_e$, and $n = n_0\ (1 - 0.8\ s + 1.3\ s^2 - 1.5\ s^3\ )$ are assumed. Central electron density, $n_0 = 1.0 \times 10^{19}$ m$^{-3}$ for (a) and $5.0 \times 10^{19}$ m$^{-3}$ for (b). Hf is the improved factor from ISS95 scaling.*

## 4. ENGINEERING DESIGN OF CFQS

### 4.1. Magnetic field coil system

Schematic view of the magnetic coil system of CFQS is shown in Fig. 5. The CFQS consists of 16 modular coils (MC, brown), 4 poloidal field coils (PFC, yellow), and 12 toroidal field coils (TFC, pink). The last-closed flux surface (LCFS) of plasma is shown in beige. A basic QA configuration can be produced by 16 MCs which have four different types in shapes. We call these 4 types of MCs as MC1, MC2, MC3, and MC4. For MCs, 4 power supply will be prepared, and the current ratio between these four types of MC can be controlled. By this control, the mirror ripple will be handled to break QA symmetry in experiments. For example, by 40 % current reduction of MC1, MC2 from original, mirror ripple component $B_{01}$ corresponding to about 20 % of $B_{00}$ can be applied. Toroidal viscosity is changed by this method to study the plasma rotation effects on the confinement. PFC is used to move the magnetic axis horizontally, and to suppress Shafranov shift of plasma. With TFC, rotational transform can be controlled by adjusting the toroidal magnetic field. Divertor configuration can be realized by using $n/m$=2/5 magnetic islands in peripheral region [30]. At the volume average $\beta$ of 0.35 %, on which bootstrap current reaches 10 kA, rotational transform increases and 2/5 magnetic islands appear in peripheral region. We can utilize this structure as island bundle divertor. Rotational transform control by TFC is another possibility to produce same 2/5 island bundle divertor.

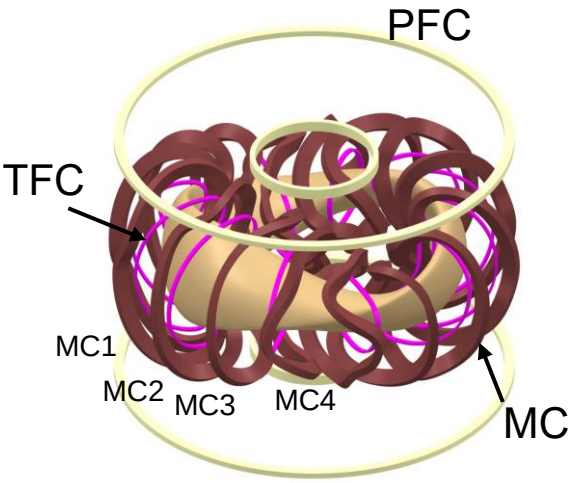


*Figure 5. Coil system for CFQS. MC: modular coils consist of MC1, MC2, MC3, MC4. TFC: toroidal field coil. PFC: poloidal field coil.*

### 4.2. Modular coils

The geometry of the conductor center of MC, the so called filament coil, is designed by NESCOIL code [31]. In the code, current carrying surface (CCS) is defined by Fourier series, on which the filament coil shape is also expressed by Fourier series. The filament coil shape with CCS geometry is optimized so that the average of normal magnetic field components, $\boldsymbol{B}\cdot\boldsymbol{n}$ / $|\boldsymbol{B}|$, produced by coils on target plasma boundary should be zero. As for engineering boundary conditions, curvature radius of filament and distance between the two adjacent coils are taken into account in this optimization. Due to the optimization of the filament coil for CFQS, the minimum distance of 18.5 cm between the adjacent coils, and the minimum radius of curvature of 21.5 cm were attained. These values are for the filament coil, and the finite size of coil cross section is not considered. For real coil system, the finite sized coil is designed so that the center of rectangular cross section should be coincided with this filament coil. Supporting structure is designed by using open space.

For the actual conductor of CFQS modular coils, hollow copper conductor having rectangular cross section are chosen, of which size is 8.5 mm × 8.5 mm. At the center of the cross section, it has a circular water cooling channel, of which the diameter is 4 mm. The total turn number of conductor for one modular coil is 12 × 6 = 72. The electric connection of these conductors is in series in one MC. Note that for the water cooling channel, the connections are in three parallel. At first, the rectangular cross section of coil was designed so that its longitudinal axis should be normal to CCS. However, in this design, the torsion and the curvature of copper conductor became high, thus the angle of the rectangular cross section along filament coil is optimized [32]. Due to this optimization, the tight curvature of the conductor was relaxed.

### 4.3. Supporting structures

The $A_p$ of CFQS is 4, this is very low value in helical devices, because $A_p$ of other typical helical devices is larger than this. For example, $A_p$ of CHS, LHD, HSX and W7-X are 5, 6, 8 and 11, respectively. Moreover, the coil

shape is intrinsically three-dimensional. Low $A_p$ makes engineering design relatively harder than other devices. Since the torus central region is very narrow due to low $A_p$, the distance between coils is short, which causes the large electromagnetic force on coil. Therefore, strong supporting structure is required although space is limited. Moreover, as a good experimental device, providing enough space for diagnostic and heating systems are desired. We have to consider this contradictory requirement in design of supporting structure. Taking these conditions and requirements into account, we designed supporting structure as shown in Fig. 6 (a) and (b). It is noted that these are current design, and some improvement/modification will be applied in the future.

As described above, CFQS is compact in size, *i.e.*, $R$ = 1 m and $A_p$ = 4, thus space available for supporting structures. To support modular coil conductors by limited space, coil case with the thickness of 10 mm are used for reinforcement, because copper conductor itself cannot stand such great electromagnetic force. To avoid interference between modular coils and vacuum vessel, U-shape coil case is designed as shown in Ref 34. Therefore, on the coil surface of vacuum vessel side, coil case does not exist, and on other three coil surfaces, coil cases reinforce conductors. Including insulation materials, and FRP spacers between conductors and coil case, total size of coil cross section with coil case is 152 mm × 99 mm for MC1, MC2, MC3, and 155 mm × 105 mm for MC4.

In the torus center, the center pillars are located and support all modular coils from the inboard side. Cage-like supporting structure supports all MCs with coil case and center pillars. In order to estimate stress on this supporting structure during 1 T operation, finite elements method (FEM) analysis was performed by ANSYS Maxwell and Mechanical. The distribution of the Von Mises stress on supporting structure is shown in Fig. 7 (a) and (b). The maximum stress is about 140 MPa, which is an acceptable level for supporting structure to withstand large electromagnetic force in 1 T operation [33, 34]. Deformation of coil conductors during 1 T operation is about 1 mm, as shown in Fig. 7 (c). This order of deformation does not make a significant effect on magnetic field configuration [37].

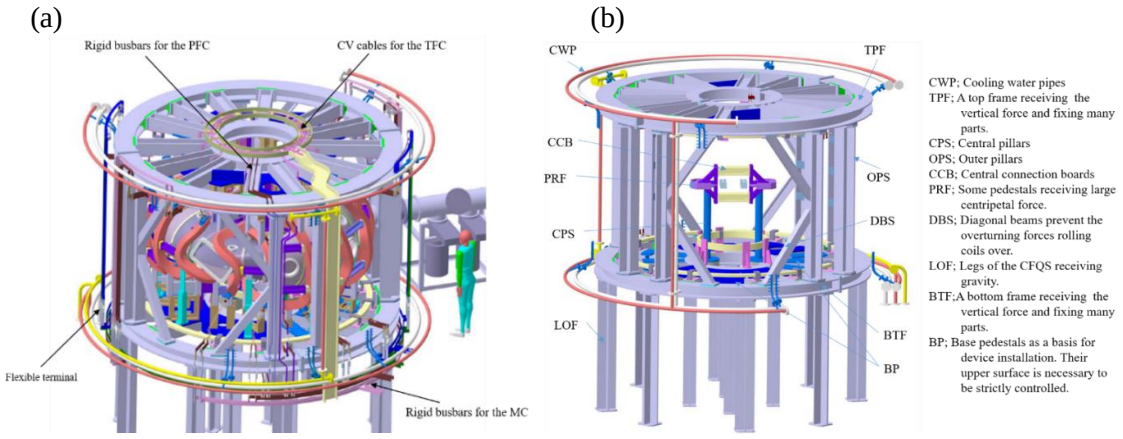


*Figure 6. (a) Supporting structure of CFQS with coil system and vacuum vessel. (b) Main supporting structure without coil system.*

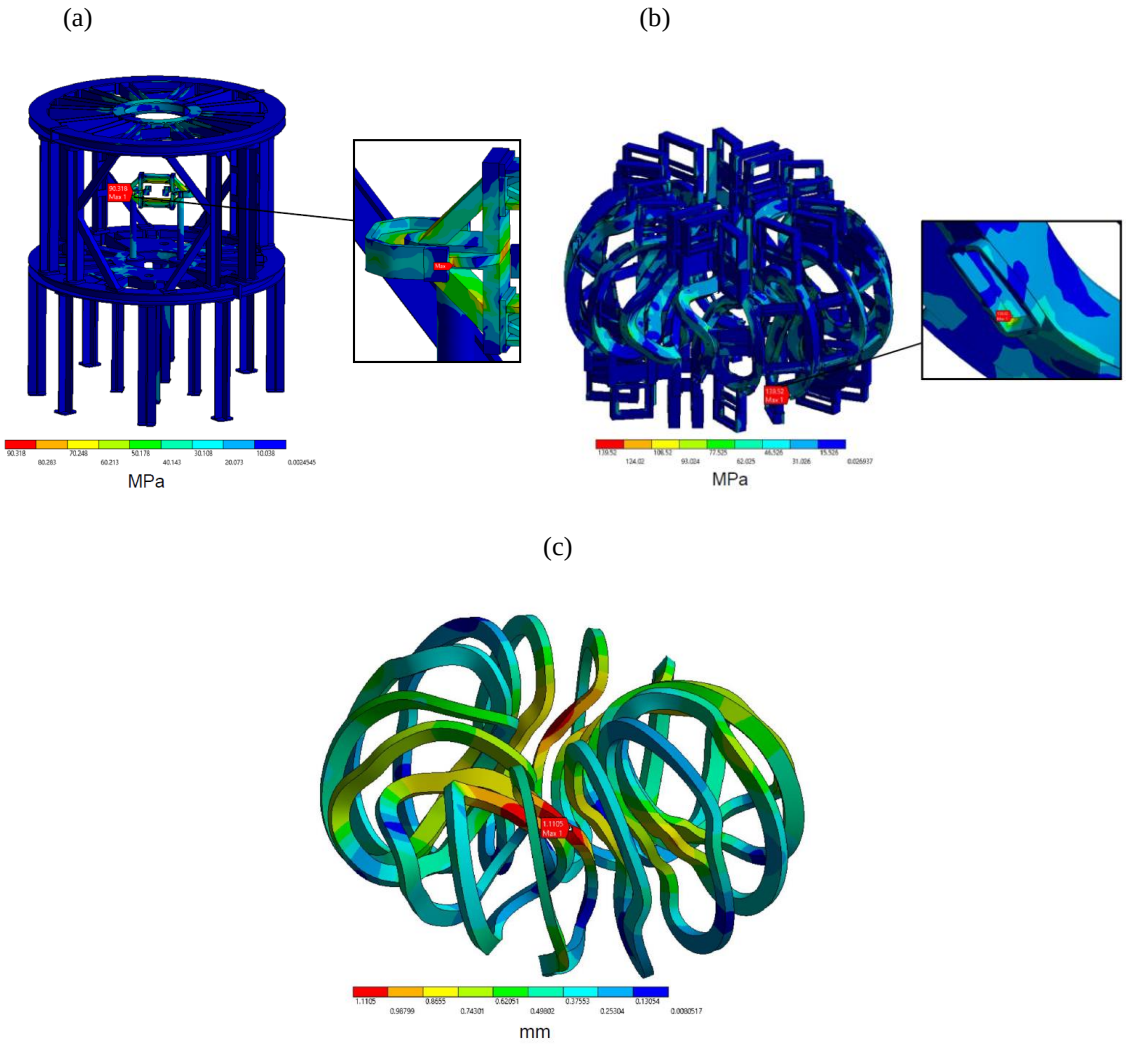


*Figure 7. Distribution of Von Mises stress (MPa) on (a) cage-like supporting structure, and (b) coil case. Unit is MPa. (c) Distribution of deformation (mm) of coil conductors.*

### 4.4. Vacuum vessel

Fig. 8 (a) shows a schematic view of the main vacuum vessel (VV), which will be manufactured by welding together four sections of two types (type A and type B) in the toroidal direction. The flanges used for welding these four sections are also shown in the figure. More than 42 large ports with a diameter of at least 114 mm, will be provided for heating and diagnostic systems as shown in Fig. 8 (b), (c), and (d). Two of them are large rectangular ports with an opening diameter (inner size) of 340 mm × 580 mm, both for a maintenance worker to enter, for NBI, and for Thomson scattering diagnostics. Since the electromagnetic forces on the VV are expected to be small, it will be fabricated from SUS316L with thickness of 6 mm. Eddy current induced in VV during operation of magnetic field coils was analyzed by ANSYS Maxwell. The time constant ($\tau$) for eddy current life time is about 4 ms. Therefore, if the plasma is produced later than 20 ms (5τ) after the beginning of flat top of coil current, the effect of eddy current on magnetic configuration can be negligible [35]. From this analysis, the one-turn resistance is evaluated, and it is roughly 0.3 mΩ. This is sufficiently high not to produce significant Joule heating.

The main VV is fixed on eight leaf-type legs, which can deform to absorb the VV's thermal expansion during baking. The VV also has twelve winding bobbins to wind the TFCs. The VV wall will be conditioned by baking

at the temperature of 130 ~ 150 ℃ with sheath heaters. FEM analysis with ANSYS Mechanical was performed to validate the reliability of VV. In this analysis, atmospheric pressure and self-weight are taken into account. Thermal load by baking is also considered. Fig. 9 (a) and (b) show distribution of Von Mises stress and deformation of VV, respectively. The analysis indicates that the maximum of Von Mises stress and deformation are 126 MPa and 3 mm respectively, which are below allowable level [36].

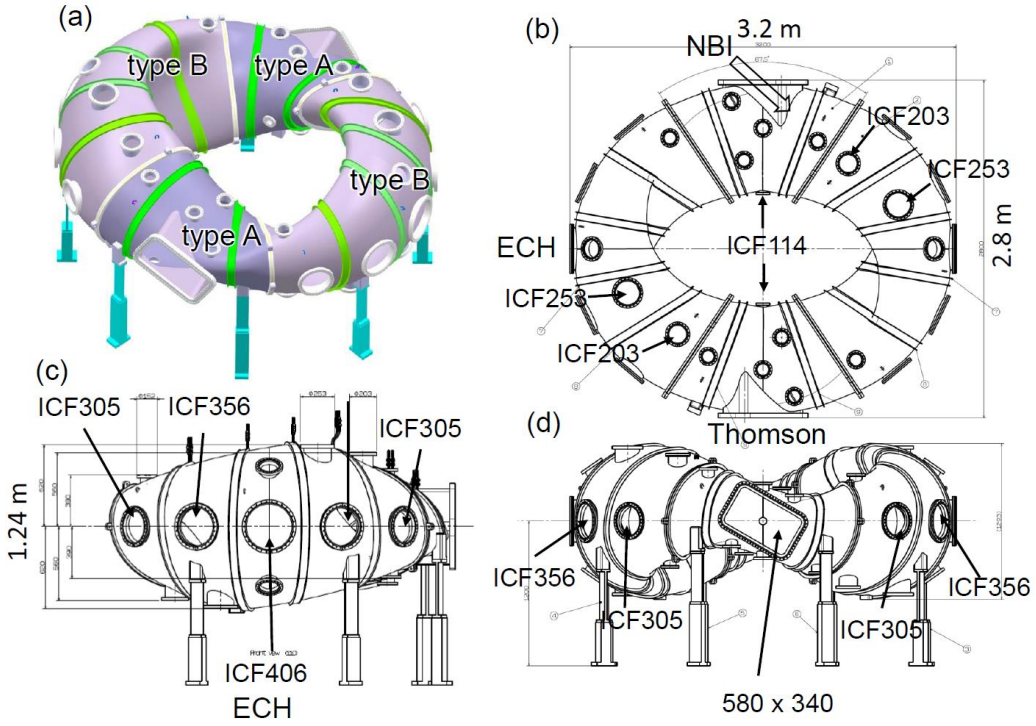


*Figure 8.* (a) *3-D model of vacuum vessel. Port arrangement on vacuum vessel, (b) top view, (c) side view at* $\phi$ *= 0 degree, and (d) side view at* $\phi$ *= 90 degrees.*

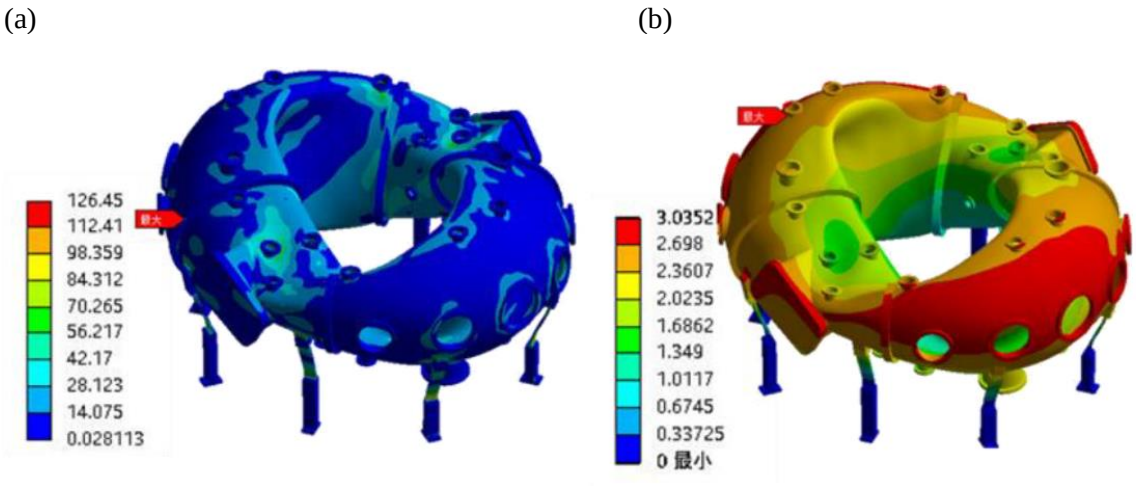


*Figure 9. (a) Von Mises stress distribution on VV, and (b) deformation distribution of VV.*

## 5. CONSTRUCTION OF CFQS

### 5.1. Mock-up of MC

In order to check the manufacturability and the accuracy of the MC, a mock-up of the MC4, which is the most complicated in shape, was constructed by the manufacturing company Hefei Keye Electro Physical Equipment Manufacturing Co., Ltd. in China. The construction process of mock-up MC4 is shown in Fig. 10. At first, mould for conductor winding was fabricated. Along this mould, copper hollow conductor, which was wrapped with insulation tape for layer isolation, was wound. During the winding process, the conductors were fixed by clamps on the mould. After the completion of the winding process, conductors were wrapped with insulation tape for ground isolation, and then vacuum pressure impregnation (VPI) was performed to fix conductors. The realized accuracy was checked with a laser tracker. Measurement data were compared with 3-D CAD model, and the maximum deviation was 3.3 mm. Simple model calculation to check the effect of the coil deviation on the magnetic surface was performed, and up to the deviation of 10 mm, its effect is not significant [37]. Heat-run test was performed to check the temperature rise of conductor and cooling water. Current of 1 kA for the pulse duration of 38 s was applied in this test, of which total Joule heating energy is almost the same to that of 1 T operation, on which the current is 4.34 kA for the pulse duration of 2 s. Time evolution of temperature rise of cooling water at inlet and outlet, and those on coil surfaces are shown in Fig. 11 in this heat-run test. Flow rate of cooling water is 3.9 L/min. The rise in temperature was 40 degrees, which is an allowable level. As for the cooling water temperature, required time down to room temperature was about 10 minutes.

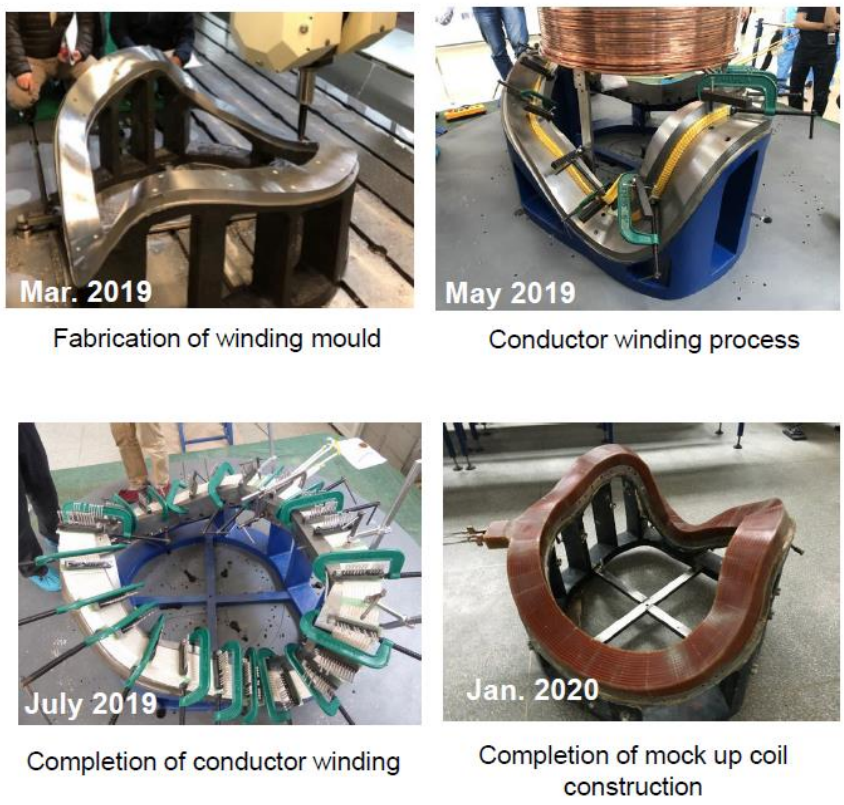


*Figure 10. Construction of mock-up MC4 which is the most complicated in shape.*

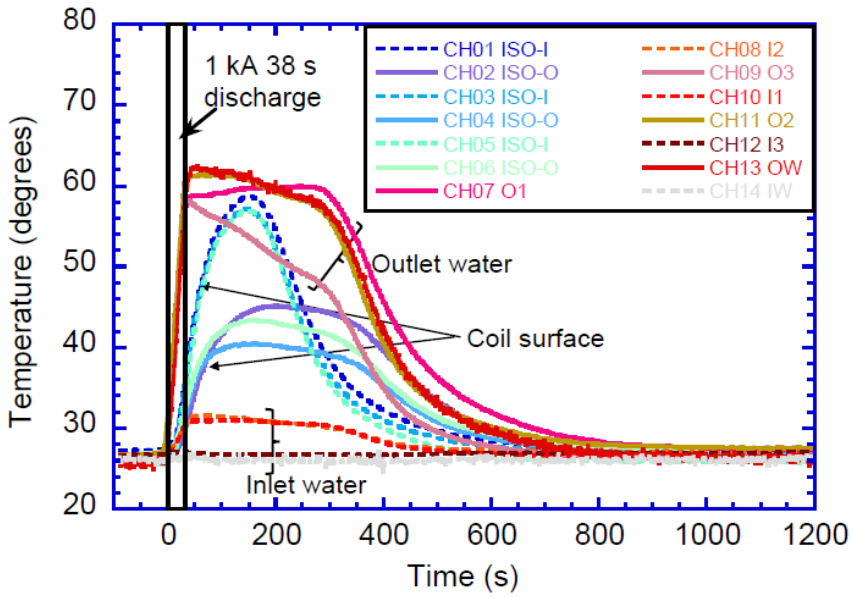


*Figure 11. Temporal evolution of coil surface and cooling water temperatures in the heat-run test for mock-up MC4. Coil current was 1 kA, and discharge duration was 38 s. Cooling water flow rate was 3.9 L/min. In legend, ISO-I, ISO-O: the temperature of coil surface at the inside and outside. I1, I2, I3, IW: the temperature of cooling water at inlet. O1, O2, O3, OW: the temperature of cooling water at outlet.*

### 5.2. Actual MC manufacturing

After the construction of mock-up MC and several tests, actual MC construction has begun. A total of 16 MCs consists of 4 independent types in shape. Therefore, 4 types of winding mould are required for the winding process. We have initiated manufacturing MC4. Fig. 12 shows the manufacturing process of MCs. In Fig. 12 (a), casting of 4 types of winding mould is shown. MC4 winding mould was precisely finalized by CNC machine as shown in Fig. 12 (b). Along this winding mould, hollow copper conductors were wound, and the first VPI was performed to fix conductors. Then, 2nd MC4 (MC4-2) was wound on this mould sequentially as shown in Fig. 12 (c). After all of 4 MC4 are wound and the first VPI for them is performed, the following process is planned. The coil, which is removed from the winding mould, will be wrapped with an insulation tape for ground isolation. Total thickness of wrapped tapes reaches 3 mm, therefore, the mould will be cut by 3 mm, and then the coil will be put on the mould once more. Subsequently, the second VPI will be performed by using this mould.

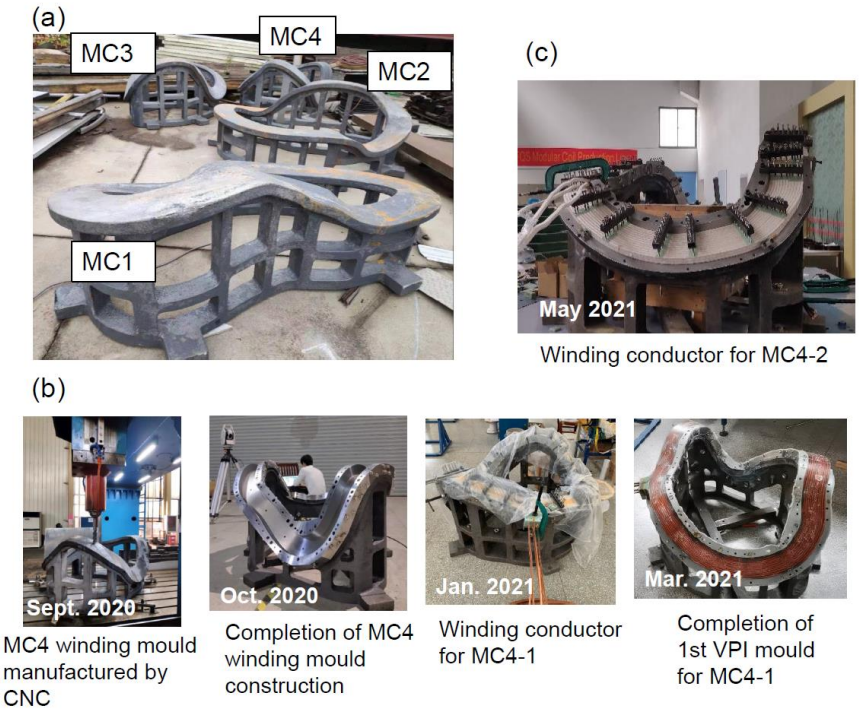


*Figure 12. (a) Winding mould for 4 different types of MCs. (b) Processes of MC4-1 construction. (c) MC4-2 winding process.*

### 5.3. Vacuum vessel manufacturing

At present, 1/4 of the toroidal section of VV is being manufactured. In Fig. 13 (a), 3-D CAD model of 1/4 toroidal section of VV is shown. To produce the complicated geometry of this VV, the 6 mm SUS plate is manufactured by press work. 1/8 toroidal section of VV is divided into 4 parts of the plate as shown in Fig. 13 (b), and one of them (part 1 plate) now begins to be manufactured. For the press work for the part 1 plate, mould for this purpose was designed and produced as shown in Fig. 13 (c) and (d). Because we have experienced significant spring back in this press work, hot pressing method is required to manufacture plates to construct VV. Moulds for other parts were already constructed as show in Fig. 13 (e). After all 4 parts of plates are manufactured by the press work, they will be welded into 1/8 toroidal section of VV. Then, two 1/8 sections of VV will be connected by welding into a 1/4 section, after that, holes for ports will be made by cutting VV, and then, port elements, *e.g.*, pipes and flanges, will be assembled by welding on VV.

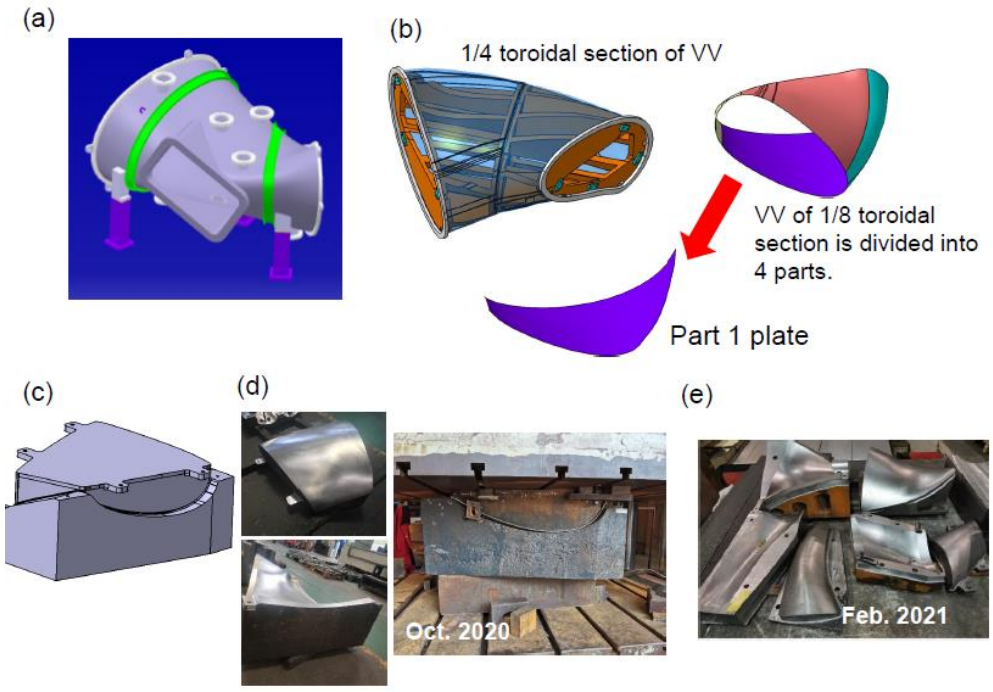


*Figure 13 (a) 3-D CAD model of 1/4 toroidal section of the VV. (b) Mould for 1/4 toroidal section of the VV, and 4 parts of 1/8 toroidal section of the VV. (c) Mould to manufacture part 1 plate by press work. (d) Photos of moulds to manufacture part 1 plate. (e) Photos of moulds to manufacture other plates.*

## 6. SUMMARY

The CFQS device is being constructed in SWJTU as a joint project of NIFS and SWJTU. Major parameters of CFQS are $R$ = 1 m, $B_t$ = 1 T, and $A_p$ = 4. CFQS has both advantages for tokamaks and helical devices due to quasi-axisymmetry. Finite beta equilibrium including neoclassical bootstrap current is investigated by the HINT 2 code. Clear magnetic surfaces are kept up to $<\beta>$ of 1.2 %, which is attainable by NBI. Coil system of CFQS consists of MC, PFC, and TFC. By the control of rotational transform with bootstrap current and/or TFC, divertor configuration can be produced. Cage-like supporting structure with coil case, which can withstand large electromagnetic force generated during 1 T operation, was designed. FEM analysis to check the reliability of the supporting structure was performed, and the analysis tells us that the estimated stress is allowable range. VV having large rectangular ports for the purpose of NBI and Thomson scattering diagnostics has been designed. In order to estimate the effect of the atmospheric pressure, self-weight and baking temperature on VV, FEM analysis was performed. The analysis indicates that VV designed for CFQS is strong enough against effects of atmospheric pressure, self-weight and baking temperature.

Mock-up MC4 has been constructed successfully. Heat run test was already performed, and capability of 2 s discharge for 1 T operation was confirmed. After various tests of mock-up coil, construction of actual modular coil and VV has begun. We will steadily continue our work to achieve first plasma.

## ACKNOWLEDGEMENTS

The authors are thankful for strong support and encouragement for this project (NSJP) from former Director General Prof. Y. Takeiri of NIFS, former Vice President Prof. W.G. Zhang, and Vice President Prof. C. He of SWJTU. The authors are also grateful for the support to the NSJP from other related staff of NIFS, especially H. Takahashi, T. Oishi, and staff of SWJTU. This research is supported by programs of international collaborations with overseas laboratories (UFEX105), promotion of magnetic confinement research using helical devices in Asia (URSX401), the NIFS general collaboration project, NIFS18KBAP041, NIFS20KBAP067, NIFS20KBAE001, and “PLADyS”, JSPS Core-to-Core Program, A. Advanced Research Networks.

## REFERENCES


[1] Nishimura K., Matsuoka K. *et al*., 1990 Fusion Technology **17** 86
[2] Anderson F. S. B. *et al*., 1995 Fusion Technology **27** 273
[3] Beidler C. D. *et al*., 1990 Fusion Technology **17** 148
[4] Shinha P., Böckenhoff D. *et al*., 2019 Nuclear Fusion **59** 126012
[5] Dinklage A. *et al*., 2018 Nature Physics **14** 855
[6] Nührenberg J. *et al*., in Theory of Fusion Plasmas (Proc. Workshop Varenna, 1994), 1994 Editrice Compositori, Bologna 3
[7] Garabedian P., 1996 Physics of Plasmas **3** 2483
[8] Boozer A. H., 1980 Physics of Fluids **23** 904
[9] Shimizu A. *et al*., 2018 Plasma and Fusion Research **13** 3403123
[10] Liu H. F. *et al*., 2018 Plasma and Fusion Research **13** 3405067
[11] Isobe M. *et al*., 2019 Plasma and Fusion Research **14** 3402074
[12] Liu H. F. *et al*., 2021 Nuclear Fusion **61** 016014
[13] CFQS TEAM, "NIFS-SWJTU JOINT PROJECT FOR CFQS - PHYSICS AND ENGINEERING DESIGN VER. 3.1.", RESEARCH REPORT NIFS-PROC Series : NIFS-PROC-119 Jan. 25, 2021
[14] Matsuoka K. *et al*., 1997 Plasma Physics Reports **23** 542
[15] Okamura S. *et al*., 2001 Nuclear Fusion **41** 1865
[16] Okamura S. *et al*., 2004 Nuclear Fusion **44** 575
[17] Matsuoka K. *et al*., 2004 Fusion Science and Technology **46** 378
[18] Shaing K. C. *et al*, 1989 Phys. Fluids **B1** 148
[19] Ware A. S., Spong D. A. *et al*., 2006 Fusion Science and Technology **50** 236
[20] Suzuki Y., Nakajima N. *et al*., 2006 Nuclear Fusion **46** L19
[21] Wang X. *et al*., 2021 Nuclear Fusion **61** 036021
[22] Wagner F. *et al*., 1982 Phys. Rev. Lett. **49** 1408
[23] ASDEX Team, 1989 Nuclear Fusion **29** 1959
[24] Fujisawa A. *et al*., 1999 Phys. Rev. Lett. **82** 2669
[25] Suzuki C. *et al*., 2002 Plasma Physics Control Fusion **44** A225
[26] Ida K. *et al*., 1997 Physics Plasmas **4** 314
[27] Ogawa K. *et al*., 2019 Plasma and Fusion Research **14** 3402067
[28] Fujisawa A. *et al*., 1997 Phys. Plasmas **4** 1357
[29] Stroth U., Murakami M., Dory R. A. *et al*., 1996 Nuclear Fusion **36** 1063
[30] Okamura S. *et al*., 2020 Journal of Plasma Physics **86** 815860402
[31] Drevlak M., 1998 Fusion Technology **33** 106
[32] Li Y., *et al*., 2020 Plasma Physics and Controlled Fusion **62** 125004
[33] Kinoshita S., *et al*., 2019 Plasma and Fusion Research **14** 3405097
[34] Xiong G., *et al*., 2020 Fusion Engineering and Design **160** 112021
[35] Murase T., *et al*., 2020 Fusion Engineering and Design **161** 111869
[36] Nakagawa S., *et al.*, 2020 Plasma and Fusion Research **15** 2405066
[37] Shimizu A., *et al*., 2019 Plasma and Fusion Research **14** 3403151